Nano Research 2013, 6(9): 644–651
DOI 10.1007/s12274-013-0340-8
Research Article

ISSN 1998-0124
CN 11-5974/O4

Cotunneling transport in ultra-narrow gold nanowire bundles

Anaïs Loubat[1,2], Walter Escoffier[1], Lise-Marie Lacroix[2], Guillaume Viau[2], Reasmey Tan[2], Julian Carrey[2], Bénédicte Warot-Fonrose[3], and Bertrand Raquet[1] (✉)

[1] *Laboratoire National des Champs Magnétiques Intenses, CNRS-INSA-UJF-UPS, UPR3228; 143 avenue de Rangueil, F-31400 Toulouse, France*
[2] *Université de Toulouse, INSA, UPS, LPCNO (Laboratoire de Physique et Chimie des Nano-Objets), F-31077 Toulouse, France; CNRS; UMR5215; LPCNO, F-31077 Toulouse, France*
[3] *Centre d'Elaboration de Matériaux et d'Etudes Structurales, CNRS, 29 rue Jeanne Marvig, F-31077 Toulouse, France*

Received: 20 March 2013
Revised: 27 May 2013
Accepted: 27 May 2013

KEYWORDS
ultra-narrow gold nanowires,
1D nano-objects,
electronic transport,
variable cotunneling,
Coulomb blockade

ABSTRACT

We investigate the charge transport in close-packed ultra-narrow (1.5 nm diameter) gold nanowires stabilized by oleylamine ligands. We give evidence of charging effects in the weakly coupled one-dimensional (1D) nanowires, monitored by the temperature and the bias voltage. At low temperature, in the Coulomb blockade regime, the current flow reveals an original cooperative multi-hopping process between 1D-segments of Au-NWs, minimising the charging energy cost. Above the Coulomb blockade threshold voltage and at high temperature, the charge transport evolves into a sequential tunneling regime between the nearest-nanowires. Our analysis shows that the effective length of the Au-NWs inside the bundle is similar to the 1D localisation length of the electronic wave function (of the order of 120 nm ± 20 nm), but almost two orders of magnitude larger than the diameter of the nanowire. This result confirms the high structural quality of the Au-NW segments.

1 Introduction

Nanoscale materials turn into fascinating objects when exploring the size and shape dependence of their electronic properties. Remarkable quantum phenomena driven by an extreme electronic confinement can manifest themselves at room temperature [1]—such as Coulomb blockade or quantized conductance, to cite only a few examples. Their engineering opens innovative routes for the emergence of breakthrough technologies in conventional microelectronics relying on new physics principles [2, 3]. One-dimensional (1D) nanostructures like metallic nanowires belong to this promising class of nanomaterials [4, 5]. They have been already extensively studied as molecular-scale interconnects [6], biosensors [7] or waveguides [8].

Address correspondence to Bertrand.Raquet@lncmi.cnrs.fr

Noble metals, such as gold, are attractive since they are chemically inert, low resistive, highly crystallized in a simple face-centered structure, with a modest melting point and a self assembling nature. Over the last decade, tremendous efforts have been developed to fabricate high quality Au-NWs. Let us cite, among others, the standard top-down approach based on electron-beam lithography with post-fabrication downsizing by electrochemical or dry etching [9], the direct electron beam writing in Au nanocrystal films [10] or the electrochemical reduction or deposition within porous templates [11, 12]. These techniques usually produce thick (> 10 nm diameter), polycrystalline wires with diffusive surfaces [9]. With the gold Fermi wavelength being of the order of a few Ångstroms, quantum confinement phenomena in such wires are obviously absent even at the lowest temperatures. Only recently, sub-2-nm diameter single crystal Au-NWs with aspect ratios larger than 2,000 have been synthesized in an organic solvent (oleylamine) acting as a reducing and shape-directing agent [13, 14]. Interestingly, if one considers, in a simple approach, an electron gas in a 2 nm diameter cylinder confinement, the transverse energy spacing reaches a few hundreds of meV and, in the case of gold, a tenth of 1D-subbands cross the Fermi energy and participate in the electronic transport. As a consequence, these ultra-narrow Au-NWs constitute a unique 1D metallic nanostructure, in between mesoscopic wires and point contacts with an ultimate atomic confinement [15]. Unfortunately, sub-2-nm diameter Au-NWs are challenging to handle and usually break into short segments during sample preparation [13, 14, 16], preventing any electronic transport study of individual NWs.

In the following, we demonstrate that the charge transport in ultra-narrow (1.5 nm diameter) Au-NWs can be addressed by measuring the current–bias voltage characteristics of small bundles of highly ordered close-packed NWs. The analysis of the $I(V)$ curves gives evidence of charging effects monitored by the temperature and the bias voltage. The current flow at low temperature is explained by a variable range cotunneling process between weakly coupled 1D segments of Au-NWs. This constitutes the first experimental evidence of cooperative electron motion through a 1D assembly of nano-objects to minimize the charging energy. The variable range cotunneling process evolves into a sequential tunneling regime at high temperature. We deduce a 1D localisation length along the nanowires equal to the Au-segments, of the order of 120 nm ± 20 nm, almost two orders of magnitude larger than the diameter. This result confirms the high structural quality of the Au-NWs segments.

2 Experimental

Ultra-narrow Au-NWs were synthesized according to Huo et al. [17]. In brief, an Au(Ⅲ) precursor ($HAuCl_4 \cdot 3H_2O$, Alfa Aesar, 20 mg) was dissolved in oleylamine ($C_{18}H_{37}N$, Sigma–Aldrich, 5 mL). The resulting yellow solution was allowed to react at 25 ℃ for 36 h, resulting in a white precipitate. After separation (2,000 rpm, 2 min), the precipitate was heated at 45 ℃ for 48 h. Excess oleylamine was removed by three washing cycles (1:3 toluene/ethanol; 3,500 rpm, 10 min). Nanowires were finally stored in toluene solution (Sigma–Aldrich, 1 mL). To prevent the aggregation of gold nanowires into bundles, the toluene solution was sonicated 5 min prior to deposition. Microscopy samples were prepared by deposition of a diluted colloidal solution drop on a carbon-coated copper grid and observed on a JEOL-1400 microscope by bright field transmission electron microscopy (TEM). High-resolution transmission electron microscopy (HRTEM) images were obtained with a Tecnai F20 (200 kV) microscope equipped with a spherical aberration corrector. Figure 1(a) shows a TEM image of the Au-NWs that break into segments under the impact of the electron beam. The Au-NWs diameter is d = 1.5 nm and the length of the oleylamine spacer is around 2.7 nm. In the inset, the HRTEM image shows the (111) crystallographic planes, perpendicular to the NW axis.

For the electrical characterization, a few drops of the resulting colloidal solution were deposited on a p-doped Si/SiO_2 substrate. Physisorbed organic molecules were removed with toluene, and the sample was then dried under nitrogen flow. Small bundles of nanowires were localized using an atomic force microscope and connected through micro Ti/Au electrodes in a two-probe configuration separated by 3–5 μm (Fig. 1(b)). The electrodes were patterned by

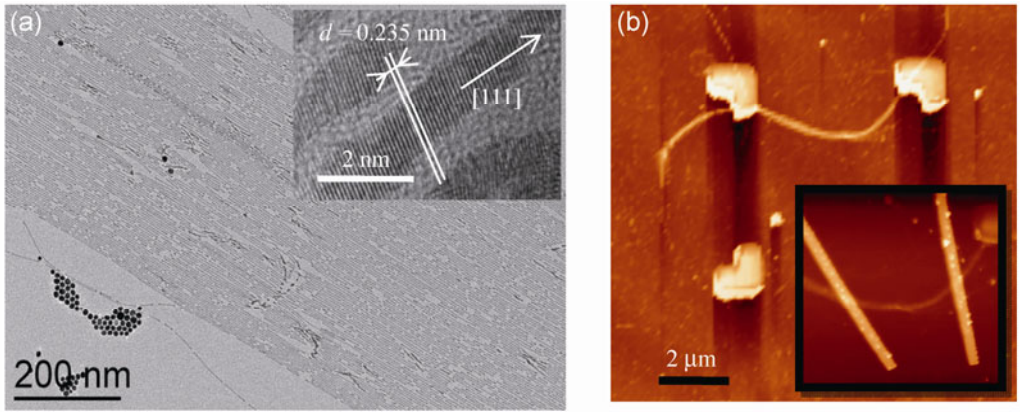

Figure 1 (a) TEM image of Au-NWs. Note the breaks of the NWs into segments under electron beam. The inset shows a HRTEM image of Au-NWs, showing the (111) lattice planes perpendicular to the NW axis. (b) Atomic force microscopy (AFM) imaging showing a 20 nm height bundle of Au-NWs before (main panel) and after the deposition of Ti/Au electrodes.

e-beam lithography, evaporation of metals and a lift-off process. The current–bias voltage measurements were performed by monitoring the applied voltage and measuring the current with an ultra low noise SR570 current amplifier. The measurements were carried out in a low temperature cryogenic system, with a variable temperature insert, from 314 to 1 K and under inert atmosphere (He). Four devices were measured, with resistances ranging from 200 MΩ to 1 GΩ at room temperature. Prior to plugging the devices into the variable temperature inset under the control atmosphere, some aging effects were detected with a slight positive drift of the device resistance. In the following, we focus on extended results obtained on the device presented in Fig. 1(b). The drain–source distance (L_{ds}) was 4 μm and the height of the bundle was approximately 20 nm, from which we anticipate the number of Au-NWs in the bundle section is 35 ± 5.

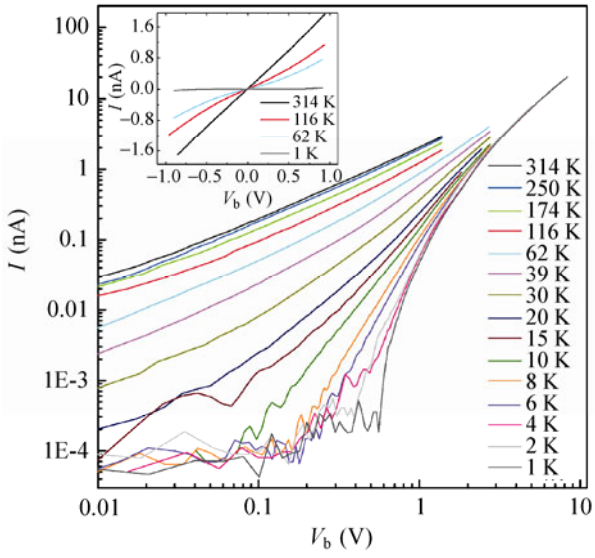

Figure 2 (Color on line) Current–voltage characteristics for selected temperatures measured on a bundle of weakly coupled ultra-narrow Au-NWs (an AFM image of the device is presented in Fig. 1(b)). In inset, $I(V)$ curves on a linear scale for selected temperatures.

3 Results and discussion

The current–voltage characteristics obtained on small bundles of ultra-narrow Au-NWs surrounded by oleylamine organic ligands were studied over a wide range of temperatures and bias voltages. In the following, we present an extended analysis of the results obtained on the Au-NWs device described in Fig. 1(b) and some characteristics of other representative devices. The $I(V)$ curves for selected temperatures are plotted in Fig. 2 (log-scale) and in the inset (linear scale). A clear ohmic regime is observed in the room temperature range while non linear I–V characteristics develop below 120 K. The 480 MΩ ohmic resistance measured at 314 K calls for some consideration.

This value is obviously orders of magnitude larger than the expected one for a multi-channel ballistic regime. On the other hand, if one considers a strongly diffusive regime along the wires, a very short electronic mean free path (L_e) in the range of the NW diameter

(1.5 nm) should be assumed as is frequently observed for narrow quasi-1D nanostructures. The resistance of a single wire of length $L_{sd} \approx 4$ μm between the contacts is then approached by the Landauer formula $R = \frac{h}{2e^2 M} \times \frac{L_{sd}}{L_e}$, of the order a few tenths of MΩ (here, h is the Plank's constant, e the electronic charge and M, the number of transverse modes). With the additional contribution of few NWs in parallel into the bundle, the assumption of a strongly diffusive regime in continuous wires yields a much smaller resistance than the experimental one. As a consequence, the large measured resistance likely originates from discontinuities in the NWs rather than an ultra-short electronic mean free path. The tunneling barriers that develop between the segmented NWs and the resulting charging effects are expected to drive the onset of the strongly non linear $I(V)$ curves as the temperature is lowered (Fig. 2).

From the $I(V)$ characteristics, we consider the temperature dependence of conductance in the low-bias voltage regime which follows a stretched exponential form, $G(T) \propto \exp\left(-\sqrt{T_0/T}\right)$, from 120 K down to 6 K, with $T_0 = 610$ K ± 10 K (Fig. 3(a)).

Below 6 K, the measured current (< 0.1 pA) cannot be extracted from the background noise of the experiment. Above 120 K, the low bias conductance undergoes a gradual crossover towards an Arrhenius behavior, $G(T) \propto \exp(-U_0/kT)$, with $U_0/k = 110$ K ± 10 K (inset Fig. 3(a)). The functional form, $\exp\left(-\sqrt{T_0/T}\right)$, usually reveals a Variable Range Hopping (VRH) conduction regime [18, 19], which manifests itself in a wide variety of poorly conducting materials [20] and results from a compromise between tunnel distances and energy costs. However, such an interpretation arouses controversial debates since very distinct mechanisms may give rise to the same temperature dependence. Let us cite the VRH in disordered semiconductors in presence of Coulomb interaction (the Efros–Shklovskii model) [19], the quasi-1D VRH in polymers [21] and the hopping regime in granular systems with specific size (capacitance) and tunnel distance distributions [22, 23]. The application of the E–S model has been extended to the hopping transport in closely packed nanoparticles [24–26], considering that an electron

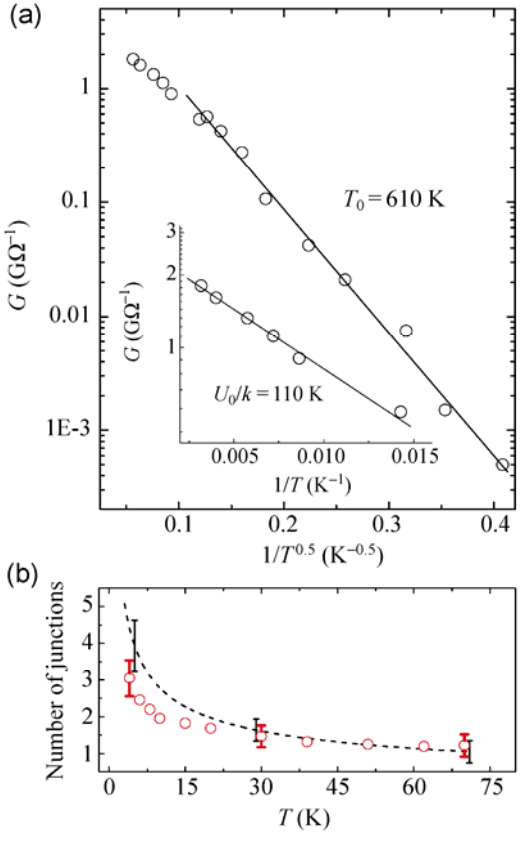

Figure 3 (a) The logarithm of the low bias voltage conductance (measured at 200 mV) plotted as a function of the $1/\sqrt{T}$, unveiling the E–S type transport regime in the Au-NWs bundle. The inset shows the high temperature dependence above 120 K, following a thermally activated behavior. (b) Dashed line: The number of tunnel junctions versus temperature deduced from the analysis of the conductance in the low bias voltage regime (Eq. (3)). Red circle symbols: The number of junctions deduced from the $I(V)$ curves in the intermediate voltage range (see Fig. 4).

optimizes a probability of thermally overcoming $1/r$ Coulomb interactions between nanoparticles (i.e., the localized states) and a probability of tunneling between nanoparticles. However, extension of the E–S model to granular systems yields unrealistically large tunneling and hopping distances for which the effective strength of the Coulomb interaction between the initial and final states is questionable [27]. Recently, a new ingredient has been successfully introduced: Multiple inelastic cotunneling processes [28, 29], reconciling E–S type conductivity with the electron hopping to the nearest-neighbors. The inelastic cotunneling event [30] involves a cooperative motion of different electrons through several tunnel junctions at a time. At a given temperature, the conductance results

from an optimized number of tunnel junctions for a cotunneling process as a compromise between a reduced charging energy cost and the drop of the transmission probability for high-order cotunneling processes. While this approach has only been considered for spherical nanoparticle arrays, in the following, we bring evidence that this concept, with some refinements, is robust enough to describe the electronic transport through highly ordered close-packed Au-NWs in bundles.

The characteristic temperature T_0 of the low-bias voltage conductance is defined by

$$T_0 = C_{\text{num}} \frac{E_C \times (L/2)}{k_B \xi} \quad (1)$$

where $L/2$ is half the length of the Au-NW (substituting the radius for spherical particles in [31]), ξ is the localization length, E_C the NW charging energy and C_{num}, a numerical factor equal to 2.8 [19]. The charging energy for weakly coupled wires is approximated by

$$E_C = \frac{e^2}{C} = \frac{e^2}{2\pi\varepsilon_r\varepsilon_0 L} \times \ln(2L/d) \quad (2)$$

where ε_r is the relative dielectric constant of oleylamine and d, the diameter of the wire. One notes that, contrary to previous studies of arrays of spherical nanoparticles [31, 32], the experimental determination of T_0 from $G(T)$ does not allow a direct determination of the localization length, since here, the total length of the NWs (L), inside the connected bundle, remains unknown. On the other hand, the analysis of the thermally activated behavior of the conductance observed at higher temperature gives additional information: The Arrhenius behavior supplants the multi cotunneling process and is characteristic of nearest-hopping between NWs. It is well known that, in a network of weakly coupled metallic dots in the Coulomb blockade regime, an optimal electronic path develops to avoid the highest charging energy cost originating from size or charge disorders. This gives rise to a relevant activation energy U_0, being a fraction of E_C in the range of $U_0 \approx 0.2 \times E_C$ [33]. From the measured value, $U_0/k = 110\ \text{K} \pm 10\ \text{K}$, we thereby approximate $E_C \approx 550\ \text{K} \pm 50\ \text{K}$, which implies a NW segment length L of 120 nm ± 20 nm. Note that the error-bar is indicative of the range of NW lengths consistent with the electronic transport. But it cannot be compared to the dispersion observed on the TEM image (Fig. 1(a)) since the electron beam for the observation severely damages the ultra-narrow Au-NWs. From Eq. (1), we finally infer an electronic localization length comparable to the NW segment length, $\xi \approx 1.1 \times L$. This means that the electronic wave functions remain localized within a NW segment. This is indeed the required condition for tunneling between weakly coupled nano-objects. Note that a rough estimate of the tunnel decay κ across the oleylamine barrier defined by $\kappa = \sqrt{\hbar^2/(2m_e\phi)}$ strengthens this scenario: Assuming a work function $\phi \approx 1$ eV, we infer $\kappa \approx 0.18$ nm, much smaller than the 2.7 nm inter-NW separation.

At a given temperature, the extent of the cotunneling events r^*, i.e., the optimal hopping distance maximizing the E–S hopping probability, is given by [31]

$$r^* = \left(\frac{E_C \xi L}{2k_B T}\right)^{1/2} \quad (3)$$

In Fig. 3(b), we plot the number of tunnel junctions $\left(j \approx \frac{r^*}{L}\right)$ participating in a single cotunneling as a function of the temperature (dashed line). It starts from approximately 4 at low temperatures and approaches a single junction in the upper temperature limit of the E–S like regime. This is fully consistent with nearest-hopping process that develops above 120 K.

We next consider the bias voltage dependence of the conductance above the ohmic regime. For intermediate bias voltages, when eV_b is much larger than $k_B T$ but when the voltage drop on each Au-segment remains smaller than the charging energy $\left(\frac{eV_b}{N} < E_C\right)$, the cotunneling regime yields to power law $I(V)$ curves with an exponent directly related to the number of tunnel junctions involved in the cooperative process, $I \propto V^{2j-1}$ [31]. Here, the number of Au-segments between the drain and source contacts is approximately $N = L_{sd}/L \approx 33$.

This defines the upper voltage limit of validity of the power law as roughly 1.5 V. Figure 4(a) presents the measured $I(V)$ curves (symbols) in the intermediate

bias voltage for selected temperatures in the cotunneling regime as well as the functional form $I \propto V^{\alpha(T)}$ in solid lines.

The experimental data are well reproduced by adjusting the α exponent. We deduce the expected number of tunnel junctions involved in the cotunneling process from $\alpha = 2j-1$ (red circle symbols, Fig. 3(b)), which are directly compared to the extracted one (dashed line) from the optimal hopping distance r^* (Eq. (3)). The two sets of data follow the same trend with a reasonable quantitative agreement. We conclude that the consistency of the analysis, in both the low and intermediate bias voltage regimes, reinforces the validity of the optimized cotunneling process at low temperature.

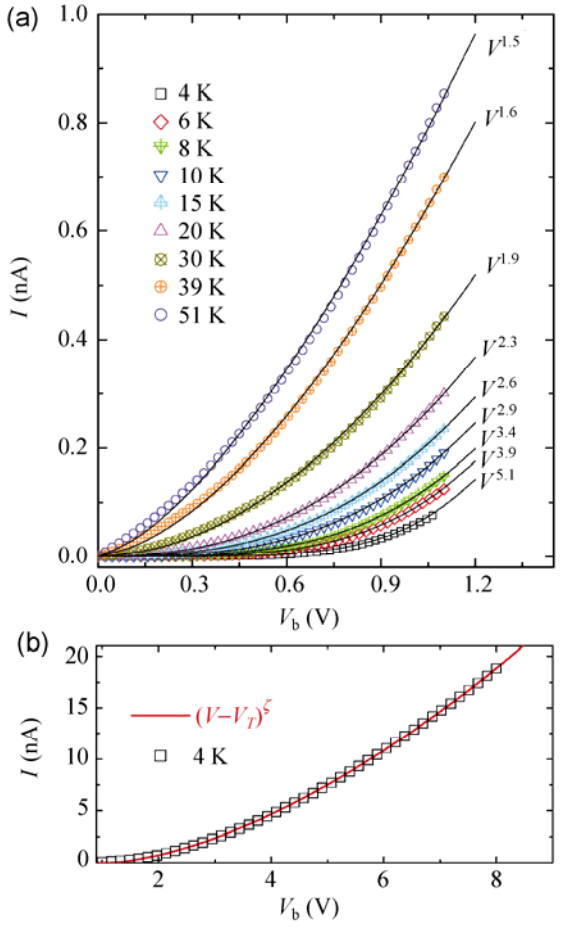

Figure 4 (color on-line) (a) $I(V)$ curves in the intermediate bias voltage range and for selected temperatures (symbols) measured on the Au-NWs bundle. The solid lines are the $V^{\alpha(T)}$ power laws. (b) $I(V)$ curve at 4 K and in the high bias voltage regime (square symbols) and the red line is the $(V_b - V_T)^\zeta$ functional form (see text).

Finally, we address the high bias voltage behavior (Fig. 4(b)), when charging effects are overcome by the applied voltage and the cotunneling process does not hold any more to reduce the charge energy cost. Following the Middleton and Wingreen (MW) model [34], the current flow in weakly coupled nanocrystal arrays percolates via local minimal Coulomb blockade thresholds and follows a single power law $I \propto (V - V_T)^\zeta$ (Eq. (4)) when $V \gg V_T$. Here, V_T is the global threshold voltage defined by $eV_T \approx \beta N E_C$, where β is a numerical pre-factor and ζ a temperature independent exponent, both depending on the geometry [34, 35]. In our case, the assumption of weakly coupled NWs is fully justified since the mutual capacitance between the Au-NWs is much smaller than the self capacitance [36]. At 4 K, the experimental $I(V)$ curve (square symbols) is well reproduced by Eq. (4) (red solid line) with V_T = 1 V and ζ = 1.63 (Fig. 4(b)). Considering $E_C \approx 550$ K and $N \approx 33$, a threshold voltage of 1 V implies a β pre-factor around 0.6. This value approaches the calculated one for a weakly coupled array ($\beta \approx 0.5$ for a dimensionality $d = 1$ and 0.338 for $d = 2$) [34]. The ζ exponent, around 1.6, also falls into the range of experimental values $1 < \zeta < 3$ and the simulated ones ($\zeta = 1$ for $d = 1$ and 5/3, for $d = 2$) [35].

4 Conclusions

Our analysis, merging the low, intermediate and high bias voltage regimes, over an extended temperature range, gives a consistent picture of an electronic transport through discontinuous, closely stacked but weakly coupled Au-NWs forming a bundle. At low temperatures, we demonstrate that the Coulomb blockade regime below its voltage threshold is conducting via a cooperative multi-hopping process. Our analysis allows extracting both the electronic localization length and the Au-NW segment length. These two dimensions are comparable, around 120 nm ± 10 nm. On the one hand, the presence of tunneling junctions along the current path is validated and gives a strong indication that the NWs are shortened into segments during the device fabrication. On the other hand, considering the ultra-narrow diameter (1.5 nm), it is remarkable to measure an electronic wave function

fully delocalized over the 120 nm segment length. This strongly supports the high crystallinity of the Au-NWs segments with a rather weak contribution of the electronic scattering at their surface.

We want to stress out that the E–S like electronic transport based on optimized cotunneling events has been theoretically developed [30] and experimentally evidenced [32, 33] for assemblies of spherical nanoparticles. Here, the formalism has been successfully adapted to a bundle of ultra-narrow Au-NWs. Nevertheless, the dimensionality of the electronic transport in our system remains an open conceptual question. The nano-objects are quasi-1D; the hopping on surrounding nearest-neighbors is possible but the optimized hopping distance via the cotunneling process is much larger than the bundle diameter, so it involves cooperative multi-electron hops mainly aligned along the bundle. Such a geometry, with a few highly ordered 1D NWs in a thin bundle, has not been theoretically addressed yet and certainly deserves dedicated charge effect simulations.

Acknowledgements

Device preparations were carried out at Laboratoire d'Analyse et d'Architecture des Systèmes (LAAS). Part of this work is supported by European Magnetic Network (EuroMagNET), contract No. 228043 and the French network French acronym for Transmission Electron Microscope and Atomic Probe (METSA). The authors acknowledge the financial support of the Laboratoire d'excellence Nano Mesures Extrêmes Théorie (Labex NEXT), No. 11 LABX 075.

References

[1] Imry, Y. *Introduction to Mesoscopic Physics*; Oxford University Press: Oxford, 2002.

[2] Appell, D. Nanotechnology: Wired for success. *Nature* **2002**, *419*, 553–555.

[3] Lu, W.; Lieber, C. M. Nanoelectronics from the bottom up. *Nat. Mater*. **2007**, *6*, 841–850.

[4] Wang, Z. L. *Nanowires and Nanobelts*: *Materials, Properties and Devices*; Kluwer Academic Publishers: Boston, 2003.

[5] Xia, Y. N.; Yang, P. D.; Sun, Y. G.; Wu, Y. Y.; Mayers, B.; Gates, B.; Yin, Y. D.; Kim, F.; Yan, H. Q. One-dimensional nanostructures: Synthesis, characterization, and applications. *Adv. Mater*. **2003**, *15*, 353–389.

[6] Wang, C.; Hu, Y. J.; Lieber, C. M.; Sun, S. H. Ultrathin Au nanowires and their transport properties. *J. Am. Chem. Soc.* **2008**, *130*, 8902–8903.

[7] Patolsky, F.; Lieber, C. M. Nanowire nanosensors. *Mater. Today* **2005**, *8*, 20–28.

[8] Barrelet, C. J.; Greytak, A. B.; Lieber, C. M. Nanowire photonic circuit elements. *Nano Lett.* **2004**, *4*, 1981–1985.

[9] Shi, P.; Zhang, J. Y.; Lin, H. Y.; Bohm, P. W. Effect of molecular adsorption on the electrical conductance of single Au nanowires fabricated by electron-beam lithography and focused ion beam etching. *Small* **2010**, *6*, 2598–2063.

[10] Jacke, S.; Plaza, J. L.; Wilcoxon, J. P.; Palmer, R. E.; Beecher, P.; De Marzi, G.; Redmond, G.; Quinn, A. J.; Chen, Y. Charge transport in nanocrystal wires created by direct electron beam writing. *Micro Nano Lett.* **2010**, *5*, 274–277.

[11] Song, J. H.; Wu, Y.; Messer, B.; Kind, H.; Yang, P. Metal nanowire formation using $Mo_3Se_3^-$ as reducing and sacrificing templates. *J. Am. Chem. Soc*. **2001**, *123*, 10397–10398.

[12] Liu, J.; Duan, J. L.; Toimil-Morales, M. E.; Karim, S.; Cornelius, T. W.; Dobrey, D.; Yao, H. J.; Sun, Y. M.; Hou, M. D.; Mo, D.; Wang, Z. G.; Neumann, R. Electrochemical fabrication of single-crystalline and polycrystalline Au nanowires: The influence of deposition parameters. *Nanotechnology* **2006**, *17*, 1922.

[13] Halder, A.; Ravishankar, R. Ultrafine single-crystalline gold nanowire arrays by oriented attachment. *Adv. Mater*. **2007**, *19*, 1854–1858.

[14] Pazos-Perez, N.; Baranov, D.; Irsen, S.; Hilgendorff, M.; Liz-Marzan, L. M.; Giersig, M. Synthesis of flexible, ultrathin gold nanowires in organic media. *Langmuir* **2008**, *24*, 9855–9860.

[15] Lagos, M. J.; Sato, F.; Autreto, P. A. S.; Galvao, D. S.; Rodrigues, V.; Ugarte, D. Temperature effects on the atomic arrangement and conductance of atomic-size gold nanowires generated by mechanical stretching. *Nanotechnology* **2010**, *21*, 485702.

[16] Chen, J. Y.; Wiley, B. J.; Xia, Y. N. One-dimensional nanostructures of metals: Large-scale synthesis and some potential applications. *Langmuir* **2007**, *23*, 4120–4129.

[17] Huo, Z. Y.; Tsung, Ch-K.; Huang, W. Y.; Zhang, X. F.; Yang, P. D. Sub-two nanometer single crystal Au nanowires. *Nano Lett*. **2008**, *8*, 2041–2044.

[18] Mott, N. F.; Davis, E. A. *Electronic Processes in Non-Crystalline Materials*; Oxford University Press: New York, 1979.

[19] Shklovskii, B. I.; Efros, A. L. *Electronic Properties of Doped Semiconductors*; Springer: London, 1984.

[20] Pollak, M.; Shkovskii, B. I. *Hopping Transport in Solids*; North-Holland: New York, 1991.

[21] Aleshin, A. N.; Lee, J. Y.; Chu, S. W.; Lee, S. W.; Kim, B.; Ahn, S. J.; Park, Y. W. Hopping conduction in polydiacetylene single crystals. *Phys. Rev. B* **2004**, *69*, 214203.

[22] Sheng, P.; Abeles, B.; Arie, Y. Hopping conductivity in granular metals. *Phys. Rev. Lett*. **1973**, *31*, 44–47.

[23] Mitani, S.; Takahashi, S.; Takanashi, K.; Yakushiji, K.; Maekawa, S.; Fujimori, H. Enhanced magnetoresistance in insulating granular systems: Evidence for higher-order tunneling. *Phys. Rev. Lett.* **1998**, *81*, 2799–2802.

[24] Yu, D.; Wang, C.; Wehrenberg, B. L.; Guyot-Sionnest, P. Variable range hopping conduction in semiconductor nanocrystal solids. *Phys. Rev. Lett.* **2004**, *92*, 216802.

[25] Liao, Z. M.; Xun, J.; Yu, D. P. Electron transport in an array of platinum quantum dots. *Phys. Lett. A* **2005**, *345*, 386–390.

[26] Romero, H. E.; Drndic, M. Coulomb blockade and hopping conduction in PbSe quantum dots. *Phys. Rev. Lett.* **2005**, *95*, 156801.

[27] Dunford, J. L.; Suganuma, Y.; Dhirani, A. A.; Statt, B. Quasilocalized hopping in molecularly linked Au nanoparticle arrays near the metal-insulator transition. *Phys. Rev. B* **2005**, *72*, 075441.

[28] Beloborodov, I. S.; Lopatin, A. V.; Vinokur, V. M. Granular electronic systems. *Rev. Mod. Phys*. **2007**, *79*, 469–518.

[29] Beloborodov, I. S.; Lopatin, A. V.; Vinokur, V. M. Coulomb effects and hopping transport in granular metals. *Phys. Rev. B* **2005**, *72*, 125121.

[30] Averin, D. V.; Nazarov, Y. V. Virtual electron diffusion during quantum tunneling of the electric charge. *Phys. Rev. Lett.* **1990**, *65*, 2446–2449.

[31] Tran, T. B.; Beloborodov, I. S.; Lin, X. M.; Bigini, T. P.; Vinokur, V. M.; Jaeger, H. M. Multiple cotunneling in large quantum dot arrays. *Phys. Rev. Lett.* **2005**, *95*, 076806.

[32] Tran, T. B.; Beloborodov, I. S.; Lin, X. M.; Hu, J.; Lin, X. M.; Rosenbaum, T. F.; Jaeger, H. M. Sequential tunneling and inelastic cotunneling in nanoparticle arrays. *Phys. Rev. B* **2008**, *78*, 075437.

[33] Parthasarathy, R.; Lin, X. M.; Elteto, K.; Rosenbaum, T. F.; Jaeger, H. M. Percolating through networks of random thresholds: Finite temperature electron tunneling in metal nanocrystal arrays. *Phys. Rev. Lett.* **2004**, *92*, 076801.

[34] Middleton, A. A.; Wingreen, N. S. Collective transport in arrays of small metallic dots. *Phys. Rev. Lett.* **1993**, *71*, 3198–3201.

[35] Parthasarathy, R.; Lin, X. M.; Jaeger, H. M. Electronic transport in metal nanocrystal arrays: The effect of structural disorder on scaling behavior. *Phys. Rev. Lett.* **2001**, *87*, 186807.

[36] The mutual capacitance between parallel NWs is estimated to 0.8 aF, roughly 5 times smaller than the geometrical capacitance defined in Eq. (2).